

RESEARCH ARTICLE

10.1029/2018MS001387

Key Points:

- Atmospheric black carbon aging processes in CAM5 are constrained by chamber experiments
- The calibrated model shows that coating results in net enhancement in BC forcing in spite of a reduction in BC lifetime
- Modeled BC direct radiative forcing varies up to 26% due to the uncertainties in BC aging parameterization and coating aerosol mass

Correspondence to:

Y. Wang,
yuan.wang@caltech.edu

Citation:

Wang, Y., Ma, P.-L., Peng, J., Zhang, R., Jiang, J. H., Easter, R. C., & Yung, Y. L. (2018). Constraining aging processes of black carbon in the Community Atmosphere Model using environmental chamber measurements. *Journal of Advances in Modeling Earth Systems*, 10, 2514–2526. <https://doi.org/10.1029/2018MS001387>

Received 28 MAY 2018

Accepted 3 OCT 2018

Accepted article online 8 OCT 2018

Published online 23 OCT 2018

©2018. The Authors.

This is an open access article under the terms of the Creative Commons Attribution-NonCommercial-NoDerivs License, which permits use and distribution in any medium, provided the original work is properly cited, the use is non-commercial and no modifications or adaptations are made.

Constraining Aging Processes of Black Carbon in the Community Atmosphere Model Using Environmental Chamber Measurements

Yuan Wang^{1,2} , Po-Lun Ma³ , Jianfei Peng⁴, Renyi Zhang⁴, Jonathan H. Jiang² , Richard C. Easter³ , and Yuk L. Yung^{1,2}

¹Division of Geological and Planetary Sciences, California Institute of Technology, Pasadena, CA, USA, ²Jet Propulsion Laboratory, California Institute of Technology, Pasadena, CA, USA, ³Atmospheric Sciences and Global Change Division, Pacific Northwest National Laboratory, Richland, WA, USA, ⁴Department of Atmospheric Sciences, Texas A&M University, College Station, TX, USA

Abstract The direct radiative forcing of black carbon aerosol (BC) on the Earth system remains unsettled, largely due to the uncertainty with physical properties of BC throughout their lifecycle. Here we show that ambient chamber measurements of BC properties provide a novel constraint on the crude BC aging representation in climate models. Observational evidence for significant absorption enhancement of BC can be reproduced when the aging processes in the four-mode version of the Modal Aerosol Module (MAM4) aerosol scheme in the Community Atmosphere Model version 5 are calibrated by the recent in situ chamber measurements. An observation-based scaling method is developed in the aging timescale calculation to alleviate the influence of biases in the simulated model chemical composition. Model sensitivity simulations suggest that the different monolayer settings in the BC aging parameterization of MAM4 can cause as large as 26% and 24% differences in BC burden and radiative forcing, respectively. We also find that an increase in coating materials (e.g., sulfate and secondary organic aerosols) reduces BC lifetime by increasing the hygroscopicity of the mixture but enhances its absorption, resulting in a net increase in BC direct radiative forcing. Our results suggest that accurate simulations of BC aging processes as well as other aerosol species are equally important in reducing the uncertainty of BC forcing estimation.

Plain Language Summary Following carbon dioxide, black carbon particle (BC) is the second climate warming agent in the Earth system. However, BC radiative effect in most global climate models (GCM) varies by a factor of 2. The uncertainty mainly arises from the transformation of BC in the atmosphere during its lifecycle and the corresponding treatment in models. Recently, a series of BC chamber experiments were conducted over two polluted regions around the world, Beijing, China, and Houston, USA, to characterize BC aging processes. In this study, we capitalize those direct observations to calibrate a key parameter associated with BC lifetime and physical property in a GCM. Our work also illustrates the importance of the coating materials of aged BC on its radiative and climate impacts. Hence, our study calls on the deployment of the ambient smoke chamber over more places and development of a reliable aerosol composition data set with a global coverage to better constrain the BC forcing assessment.

1. Introduction

The direct radiative forcing of atmospheric black carbon aerosol (BC) remains highly uncertain in the current climate assessment, due to the complexity of their optical properties and spatiotemporal distributions (Bond et al., 2013; Boucher et al., 2016; Jacobson, 2001). In particular, much of the uncertainty arises from the poorly understood BC aging processes, that is, BC changes in morphology, hygroscopicity, and optical properties by coating other materials (He et al., 2015; Wang et al., 2013). Laboratory studies have demonstrated that aging of BC is accompanied by enhancement of both absorption and scattering in the shortwave radiation, increase in water-vapor uptake capability, and morphology change from fractal aggregate to sphere (Liu et al., 2017; Xue et al., 2009; Zhang et al., 2008). The enhanced scattering by transparent coating is explained by an increase in particle volume and compaction of the soot core (Khalizov et al., 2009). However, those changes are complicated by the various mixing states of BC with other aerosols under different ambient conditions

(Cappa et al., 2012). More recently, an outdoor environmental chamber was deployed to investigate in situ BC aging processes and revealed that the timescales to achieve the complete BC aging are estimated to be 4.6 and 18 hr in Beijing and Houston, respectively (Peng et al., 2016). Meanwhile, the aging was characterized by an amplification of radiative absorption of BC as a factor of 2.4. Those direct observations of BC aging processes provide quantitative constraints for both regional and global climate models (GCMs) and have the potential of closing the gap between model predicted and observed effects of BC on regional radiation budget and climate (Gustafsson & Ramanathan, 2016).

GCMs often produce very different BC simulations (Koch et al., 2009), due likely to their insufficient spatiotemporal resolution, inevitable assumptions or simplifications in the processes of BC lifecycle, and biases in modeled meteorological conditions (Liu et al., 2007). One such crudely treated process in GCMs is the BC aging, which is even absent when BC is assumed to be either externally (Chin et al., 2009) or internally (Liu et al., 2012) mixed with other aerosol species in an aerosol microphysical module. A constant or e-folding timescale for BC aging is also widely used in some GCMs (Tie et al., 2005). More recently, a new aerosol scheme, the four-mode version of the Modal Aerosol Module (MAM4; Liu et al., 2016) was implemented in the Community Atmosphere Model version 5 (CAM5) to explicitly consider an individual fresh BC mode along with coemitted primary organic carbon. MAM4 calculates BC aging rates based on coagulation and condensation processes. The rate and fraction of converting BC from the primary carbon mode to accumulation mode is parameterized as a function of an assumed number of monolayers, which is considered as a tunable parameter useful for calibrating BC lifecycle. In this study, we constrain this parameter by comparing the modeled BC aging timescales with those estimated from recent ambient chamber experiments. We then assess the BC lifecycle and their direct radiative forcing in the calibrated model, with a focus on the uncertainty from the simulated BC coating materials and thickness.

Note that there are intrinsic differences in the BC aging definition and calculation between model and smoke chamber experiments. Chamber studies take a Lagrangian view of certain amount of BC particles after they are emitted into the chamber, so the instrument can track the whole processes of BC transformation. Differently, a three-dimensional model dynamically treats BC source, sink, aging, and transport under a Eulerian view. Therefore, we need to use some common thresholds to reconcile the definitions of the *completion* of BC aging in models and observations. Fortunately, the evolutions of the physical property from fresh to aged BC in MAM4 and the chamber works share some common features. In MAM4, an aged BC particle in the accumulation mode has the volume mean diameter of 220 to 280 nm, which is about twice of the newly emitted BC diameter (130 nm; Neale et al., 2012). This is consistent with the chamber experiments that assume that the coating thickness is about the same with the BC core size when aging is finished (Peng et al., 2016).

2. Method, Data, and Model Description

2.1. BC Treatment in MAM4

The aerosol module MAM4 includes a primary carbon mode, an Aitken, an accumulation, and a coarse mode. BC aging is explicitly considered by calculating condensation rates of certain gas species (H_2SO_4 , semivolatile organics, etc.) and coagulation rates with existing particles and dynamically moving the BC mass content from the primary carbon mode to the accumulation mode. Based on the hourly model output, the fresh BC aging time can be estimated as the fresh BC concentration divided by the total rate of coagulation and condensation on the fresh BC particles:

$$\tau_{\text{aging}} = \frac{q_{\text{BC, fresh}}}{\partial(q_{\text{BC}})_{\text{conden.} + \text{coag.}} / \partial t} \quad (1)$$

where q indicates mass concentration. The definition of modeled aging timescale reflects the time it takes to convert BC mass from the fresh BC mode to the accumulation mode. Note that the fresh BC aging timescale is not equal to the fresh BC lifetime, except when transports are not considered as an important sink or source term in the fresh BC budget over a large domain and during a long time period.

During the model integration, the BC aging rate mainly depends on mass concentrations of BC core and coating materials as follows:

$$\partial(q_{\text{fresh_BC}})_{\text{aging}}/\partial t = q_{\text{fresh_BC}} \cdot f_{\text{aging}}/\partial t \approx q_{\text{fresh_BC}} \cdot \left(\frac{V_{\text{shell}}}{V_{\text{core}}} / \frac{CT(m)}{D_{\text{pcar}}} \right) / \partial t \quad (2)$$

where f_{aging} is the aging mass fraction, V denotes the volume, and D_{pcar} is the geometric mean diameter of the primary carbon mode. $CT(m)$ is the coating thickness of monolayers on fresh BC, which is a product of the number of monolayers (m) of sulfate or equivalent amount of secondary organic aerosols (SOA) and thickness of a single monolayer. As shown in equation (2), the larger coating thickness with fresh BC, the less BC aging rate. The thickness of a single monolayer is set to be about 0.5 nm, which is approximately the size of SO_4 ion. As an important criterion with a fixed value in the model, the number of monolayers (m) is used to determine the fraction of BC to be aged at each time step, but its value may vary in a wide range from 0 to 8. The case $m = 0$ corresponds to the instantaneous mixing of BC with other aerosols right after BC emissions, similar to the treatment in the three-mode version of MAM. The more monolayers used, the longer time it requires to finish the BC mode switch. Currently, $m = 3$ is used for MAM7, but $m = 8$ is used for MAM4 (Liu et al., 2016).

The BC mass-weighted absorption coefficient, or mass absorption cross section (MAC), is a good metric to quantify changes in BC optical properties due to aging in an aerosol module. Hence, we define the BC absorption enhancement factor (AEF) from fresh to aged stage by the following equation:

$$\text{AEF} = \frac{\left(\frac{\beta_{\text{abs}} - \beta_{\text{abs_no_BC}}}{q_{\text{BC}}} \right)_{\text{accumulation}}}{\left(\frac{\beta_{\text{abs_BC}}}{q_{\text{BC}}} \right)_{\text{fresh}}} \quad (3)$$

where q is mass concentration and β_{abs} is absorption coefficient. The MAC of fresh BC with a volume diameter about 134 nm is $5.5 \text{ m}^2/\text{g}$ based on the parameterization of CAM5 (Ghan & Zaveri, 2007), which is consistent with the Mie calculation. Hence, $5.5 \text{ m}^2/\text{g}$ will be used in the denominator of equation (4). Note that such a theoretic value is rarely observed, because fresh BC can be quickly coated with a thin non-BC coating under ambient conditions and typically does not have a spherical shape (Bond & Bergstrom, 2006; Samset et al., 2018).

2.2. Environmental Chamber Experiment and Field Measurements

A quasi-atmospheric aerosol evolution study (QUALITY) chamber was developed recently to study aerosol properties and their evolution under ambient conditions. The QUALITY has a lower flow chamber and an upper reaction chamber, separated by a semipermeable membrane. The membrane allows unimpeded semi-penetration of ambient gases at a steady flow rate but filters out ambient particles from the lower to upper chambers. Therefore, the QUALITY chamber continuously captured the ambient gas concentrations without the presence of ambient particles (Peng et al., 2017). By introducing BC particle inside the upper reaction part of the QUALITY chamber, evolution of a variety of BC characteristics can be monitored.

The ambient experiments using QUALITY to characterize BC aging were conducted during two field campaigns under different pollution conditions. During May–June 2009, the Study of Houston Atmospheric Radical Precursors (SHARP) field campaign was conducted in Houston, Texas, which is a typical industrialized and populous urban area, to understand the primary and secondary sources of the radical precursors for aerosol and ozone formation (Olague et al., 2014). In August–September 2013, a similar field campaign was conducted in Beijing, one of the most polluted cities in China, to study the frequent severe haze events during that time period (Peng et al., 2016). Since the particulate pollutions in those two cities are not in the same level (Zhang et al., 2015), the comparison of the measurements at the two places would shed light on the BC aging features under different ambient conditions. During the two field campaigns, the BC coating thickness, effective density, hygroscopicity, and absorption coefficient as a function of exposure time were investigated concurrently using a suit of state-of-the-art aerosol instruments (Peng et al., 2016). Concurrent particulate matter chemical composition measurements were carried out using the Aerosol Chemical Speciation Monitor in Houston and aerosol mass spectrometer in Beijing during the same time periods (Guo et al., 2014; Levy et al., 2013).

2.3. CAM5-MAM4 Model Setup and Experiment Design

The recently developed CAM5-MAM4 is employed in this study. An interactive chemistry scheme based on the Model for Ozone and Related chemical Tracers (MOZART) is coupled to achieve better simulation of

Table 1
Numerical Experiment Design

Experiment purpose	Model configuration	Monolayers	Emissions	Integration time
To compare with ambient chamber measurements and to test the effect of monolayer	Transient simulations with modified CAM5-Chem nudged by reanalysis wind	3	The default AR5 emission	2008–2009, 2012–2013
		8	The default AR5 emission	2008–2009, 2012–2013
To test the sensitivity of coating effect	Climatological simulations with CAM5-Chem	3	Default	11 years
		3	$2 \times [\text{SO}_2/\text{SOAG}]_{\text{emiss}}$	11 years
		3	$3 \times [\text{SO}_2/\text{SOAG}]_{\text{emiss}}$	11 years
To test the linearity of BC effect with BC emission	Climatological simulations with CAM5-Chem	3	$3 \times [\text{BC}]_{\text{emiss}}$	11 years

Note. SOAG = secondary organic aerosol precursor gases, BC = black carbon aerosol.

aerosol precursor gases (Tilmes et al., 2015). Aerosol optical properties in each mode are calculated on the basis of wet refractive index and wet surface radius following Ghan and Zaveri (2007). Volume mixing of insoluble and soluble particles is assumed within each mode to obtain the wet refractive index for mixtures. Computation of BC direct radiative effect (DRE) is based on the *double-call* method implemented in the radiation diagnostic package in CAM5, where the radiation scheme was called with and without BC in the radiation transfer (Jiang et al., 2016). Hence, DRE is calculated as differences in net radiation fluxes at top of atmosphere (TOA) from two calls. As suggested by Forster et al. (2016), the total BC effective radiative effect (including direct, indirect, and semidirect) can be determined by changes in TOA fluxes in a set of 10-year atmospheric simulations with fixed sea surface temperature.

We will mainly examine those two options in this study by running two sets of simulations (M3 and M8). To facilitate the observation-model comparison and to reduce the uncertainty propagated from the simulated dynamical fields, the surface wind fields in the model are nudged by the reanalysis data every 6 hr (Ma et al., 2015). The model is run at $1^\circ \times 1^\circ$ resolution. Note that CAM5 does not have subgrid variability for aerosols, so we have to use the modeled results at 1° resolution to represent the regions of our interest such as Beijing and Houston for the model comparison with point observations.

Inside the environmental chamber, very limited amount of sulfate and nitrite aerosols were found, presumably due to the slow gas-phase oxidation of SO_2 on the timescale of a few hours (Peng et al., 2017). In contrast, more than 90% coating mass on BC is composed of SOA. Hence, to facilitate a realistic comparison between model and chamber studies, the condensation of H_2SO_4 and the coagulation of sulfate aerosols in accumulation and Aitken modes are turned off in the experiments of evaluating the BC aging timescale.

Biogenic and anthropogenic emissions of aerosol and precursor gases are adopted from a historical emission data set developed for the IPCC AR5 (Lamarque et al., 2010), and the present-day climatology (the year 2000) is used in our model simulations. Only the surface level BC properties in the model simulated are compared with the environmental chamber observations. After the model evaluation, we perform 10-year climatological simulations with fully functional aging processes and various emission setups (Table 1).

3. Result

3.1. Model Evaluation and Optimization From Two Campaigns

Figure 1 shows the simulations of BC aging rates and timescales during the two field campaign in Beijing and Houston using the default CAM5-MAM4 with eight monolayer configurations. Although constant emission rates are used within each month, the model shows a large day-to-day variability in BC aging rates, presumably due to the dynamical removal and transport processes of aerosols and precursor gases at each location. The mean BC aging rate in Beijing is about seven times higher than that in Houston, which is expected. However, the BC aging time estimation based on equation (1) shows that it takes 23.1 hr on average in Beijing to complete the hydrophobic-to-hydrophilic conversion, while it only takes about 8.3 hr for the same process in Houston (Figures 1c and 1d). Such a result surprisingly contradicts the ambient chamber

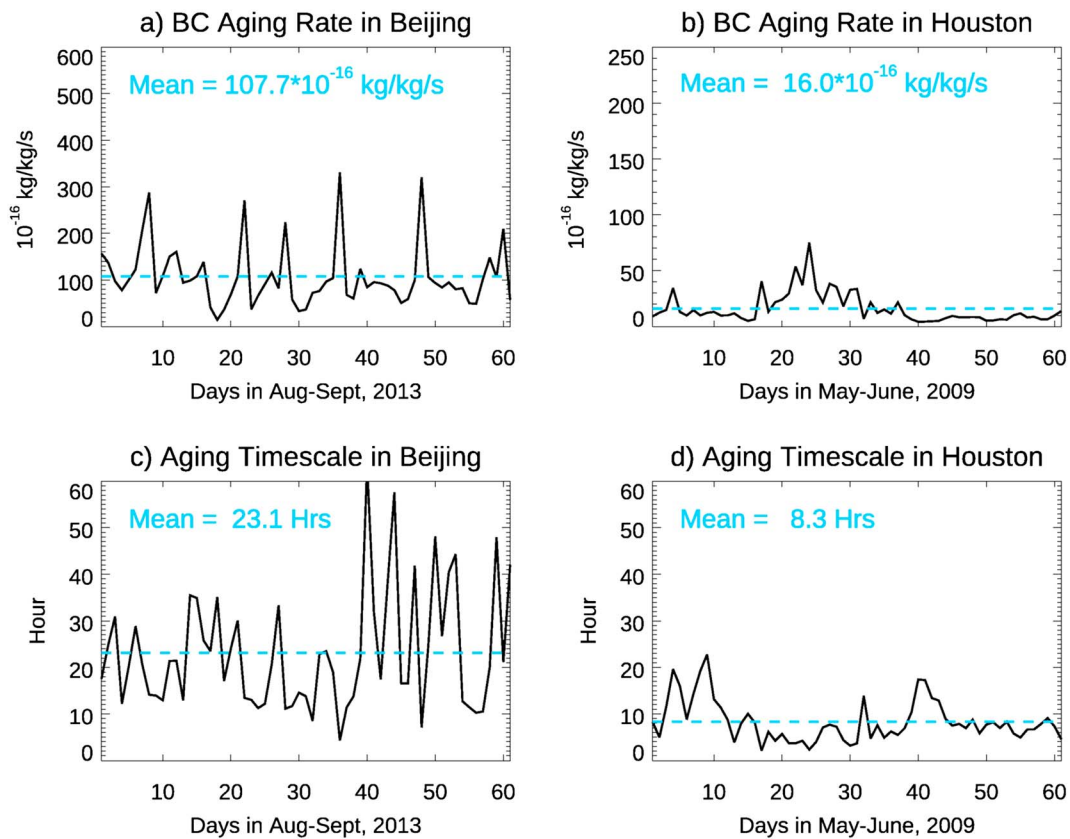


Figure 1. The default CAM5-MAM4 simulated black carbon aerosol (BC) aging rate and timescale over Beijing and over Houston during the two field campaigns.

measurements by Peng et al. (2016), which showed much faster aging process under a more polluted environment like Beijing.

To understand such a model discrepancy, we compare the simulated aerosol chemical compositions with in situ measurements, focusing on three major species of interest: BC, organic matter (OM), and inorganics as a whole. According to equation (2), the fresh BC aging rate is proportional to the volume or mass ratio between the coating shell and BC core. For our case where OM is the dominant coating material, in situ measured total BC and total OM ratio in PM₁ (particulate matter less than 1 μm) partly reflects the coating thickness per unit BC mass. Such a ratio can be further linked to the aging rate. We find that the BC:OM mass concentration ratio in Beijing (0.15) is overestimated by 60% due to the underestimation of OM in CAM5-Chem (Figure 2). In contrast, the simulated BC:OM mass ratio in Houston (0.03) is only about 1/6 of the observed value (0.17), which is attributed to the high bias in OM and low bias in BC mass concentration. Hence, the thin coating in Beijing slows down the aging rate and prolongs the aging timescale in the model. The reverse is true for Houston.

To minimize the influence of the modeled composition biases, we apply an adjustment factor (α) to our off-line aging time estimation based on the observed aerosol constituents:

$$\tau_{\text{aging_adj}} = \alpha \cdot \tau_{\text{aging}} = \frac{(q_{\text{BC}}/q_{\text{OM}})_{\text{obs}}}{(q_{\text{BC}}/q_{\text{OM}})_{\text{model}}} \cdot \tau_{\text{aging}} \quad (4)$$

We recognize that the BC:OM ratio is not an optimal scaling factor to account for the aerosol biases in the model. Given the prevalence of SOA as a coating in the smoke chamber, a more accurate factor should be BC:SOA, but an estimation of SOA mass concentration was not available for the 2009 SHARP/SOOT field campaign in Houston. By using OM instead of SOA mass concentration, we assume that the modeled SOA:OM ratio is consistent with observations. We find that such an assumption is valid at least for Beijing. During the fall season (SON), the simulated SOA:OM in Beijing is 45.5% in CAM5, which is very close to the

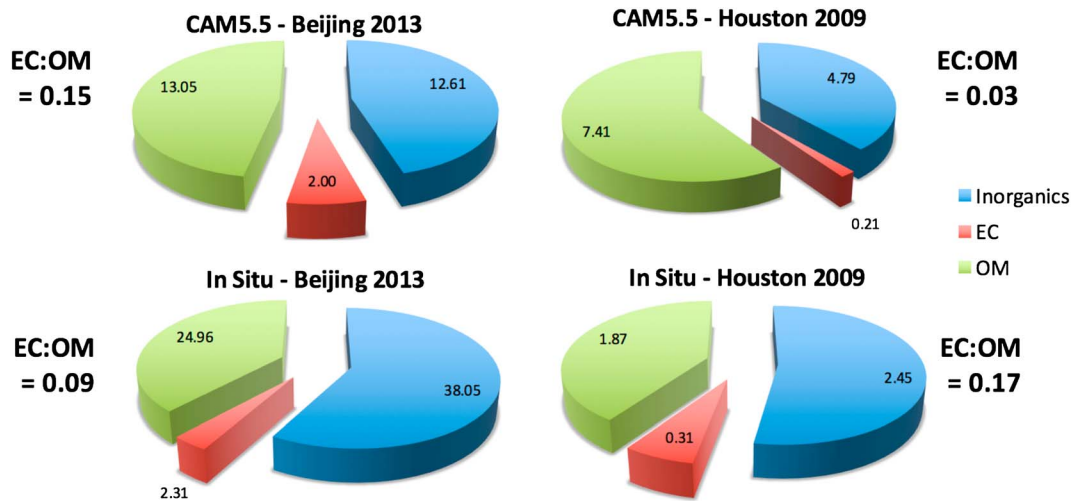


Figure 2. Major chemical compositions for accumulation mode of aerosols in CAM5-MAM4 and field measurements. The ratio of elementary carbon (EC) to organic matter (OM) is our focus as it largely reflects the coating efficiency.

observed value 47% based on the application of positive matrix factorization on aerosol mass spectrometer (Hu et al., 2017).

After applying this correction, we see a more reasonable aging-rate comparison between Beijing and Houston as shown in Figure 3. More importantly, the three-monolayer simulations (M3) show better agreement with observed aging timescale in both Beijing and Houston than those using eight monolayers (M8). Hence, we suggest that the three-monolayer can be a better choice in MAM4 to represent the BC aging criterion.

Next, we examine the optical property changes during the BC aging in CAM5-MAM4. In accordance with our previous chamber study, BC MAC is investigated here, which is measurable through a combination of different in situ instruments (Zanatta et al., 2016). Figure 4a shows the global distribution of CAM5-simulated MAC for BC-containing particles (defined as the BC mass fraction in PM1 greater than 1%) during the two campaign periods. The global mean MAC is about 16.4 m²/g, and the continental mean is about 15.6 m²/g at the visible wavelength. The measured MAC of BC-containing particles is reported to be about

11.7–13.8 m²/g in European urban areas (Laborde et al., 2013; Liu et al., 2010), 11.3–19.9 m²/g in the Indo-Gangetic Plain (Thamban et al., 2017), and 11.1 ± 2.8 m²/g in eastern China (Chen et al., 2017), after the values are converted to the 550-nm wavelength. CAM5-MAM4 model predicts mean MAC of 15.5, 14.6, and 13.7 m²/g over Europe, India, and east China, respectively. They generally agree with the observed magnitudes of BC MAC, with possible overestimation over some regions like Europe.

In CAM5, the MAC for fresh BC has a MAC of 5.5 m²/g, which is subject to the assumption of refractive index in its parameterization. Based on the AEF definition in equation (4), we find that the modeled BC AEF ranges from 1.5 to 3.5 for most regions near the BC emissions (Figure 4b), indicating strong enhancement of shortwave absorption by coating. AEF at Beijing and Houston is 2.5 and 3.2, respectively, which is generally consistent with the chamber study by Peng et al. (2016) at those two cities. The remote maritime regions tend to have a slightly higher MAC and AEF than the source regions over land. For example, the northwest Pacific has larger MAC and AEF than the upwind source region of east China. Similarly, the BC plumes received by the southwest Atlantic region are more absorbing than those in the corresponding source region near the southern Africa. This phenomenon is mainly caused by the growing

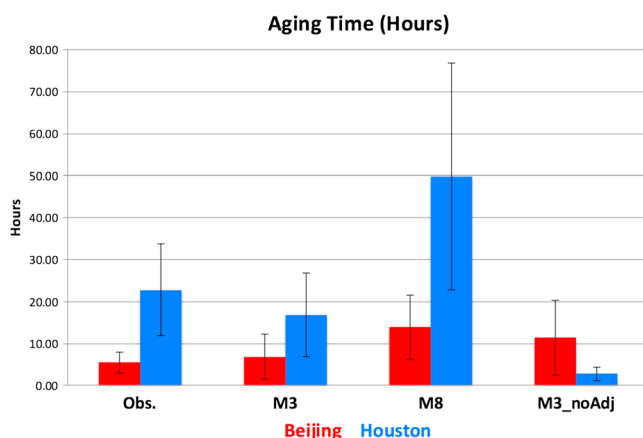


Figure 3. Comparison of mean black carbon aerosol BC aging times between CAM5-MAM4 simulations with different numbers of monolayer (M3 and M8) and observations (Obs.). The unadjusted aging time for M3 without the scaling factor (M3_noAdj) is shown as well. The error bars indicate the day-to-day variabilities.

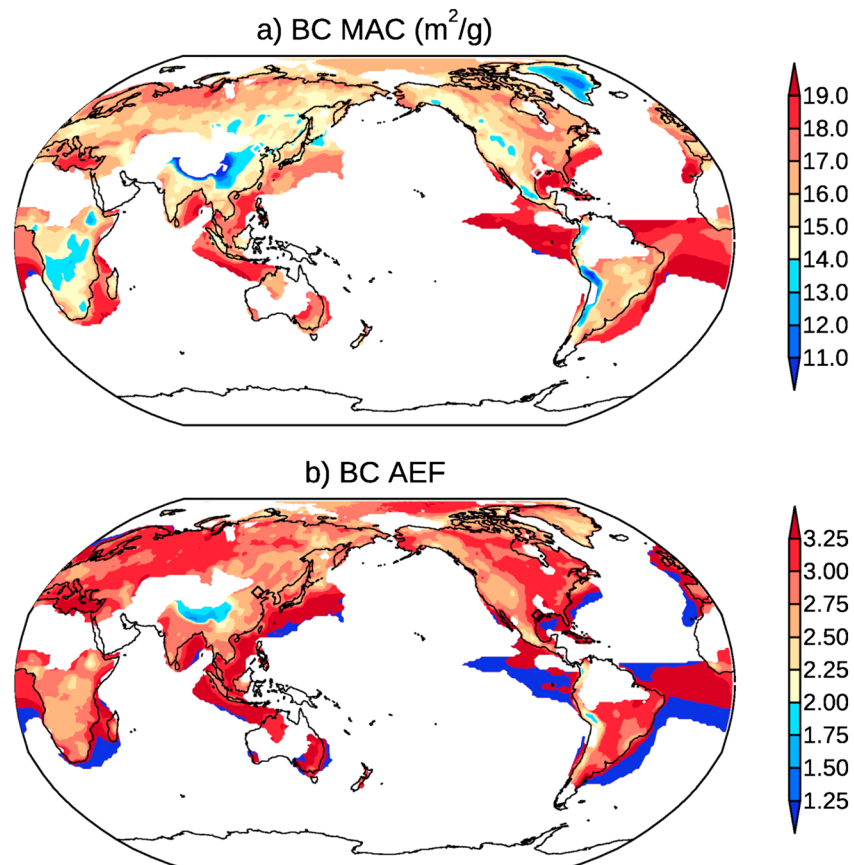


Figure 4. Global distribution of (a) mass absorption cross section (MAC) and (b) absorption enhancement factor (AEF) due to black carbon aerosol (BC) at surface level in CAM5-MAM4 for April–May, 2009, and August–September, 2013. The regions without BC-containing particles (BC mass fraction less than 1% in PM_{1.0}) are in white. The rhombuses indicate the locations of Beijing and Houston.

coating mass during transports of particles. For the same reason, the BC hotspots over land, for example, east China, north India, central Africa, and Amazon, have lower AEF than the surrounding region. We also find that the values of AEF do not change with how many monolayers we choose, indicating its independence with the BC aging speed. The model behavior agrees with the chamber measurements on the similar AEF from different ambient pollution conditions at Beijing and Houston.

3.2. Influence of Monolayer Choice

The monolayer choice is important for BC lifecycle and its climate radiative effect. We explore the sensitivity of the modeled BC properties and radiative effect to different monolayer configurations (M3 and M8) in the model climatological runs. The global mean of BC DRE at TOA in CAM5-MAM4 with the default CMIP5 emission data set is 0.46 W/m^2 , which can be caused by the systematic low biases in BC abundance in this model. In a multimodel assessment, Bond et al. (2013) suggested scaling up the modeled BC DRE by different factors at different grids based on the ratios between modeled and the AERONET measured absorbing aerosol optical depth (AAOD) values at the same month and location. However, a recent study pointed out that location biases of AERONET stations near the urban regions may cause an overestimation of AAOD (Wang et al., 2018), even though there is no doubt that the current CMIP5 anthropogenic emissions tend to underestimate BC sources. Since too many factors contribute to the current large uncertainty in the modeled BC burden in addition to BC emissions, here we decide not to tune the BC emission in our control experiment. To reveal the influence of BC emission factors on the BC properties and radiative forcing, we conduct an additional set of sensitivity experiment by scaling up BC emission rate by a factor of 3 globally, similar with Xu and Xie (2015). We find a good linearity of BC burden and absorption in response to the emission scaling. BC

Table 2

Simulated Global Mean Changes in Black Carbon Aerosol Related Properties Due to Different Monolayer Numbers and Precursor Emissions for Coating Materials

Variables	Ctrl	M8 – M3		$3 \times [\text{SOAG}]_{\text{emiss}} - \text{Ctrl}$		$3 \times [\text{SO}_2]_{\text{emiss}} - \text{Ctrl}$		$3 \times [\text{BC}]_{\text{emiss}} - \text{Ctrl}$	
		Abs.*	Frac. (%)	Abs.	Frac. (%)	Abs.	Frac. (%)	Abs.	Frac. (%)
Burden ($\mu\text{g}/\text{m}^2$)	172	41.0	23.8	-6.7	-3.9	-5.9	-3.4	373	216
AAOD	$2.6\text{e}-3$	$5.1\text{e}-4$	20.0	$5.4\text{e}-5$	2.1	$5.0\text{e}-5$	1.9	$5.4\text{e}-3$	208
Lifetime (day)	4.27	0.98	22.3	-0.16	-3.7	-0.14	-3.3	4.35	1.9
DRE (W/m^2)	0.46	0.12	26.1	0.01	2.4	0.01	2.4	1.24	169
DREC (W/m^2)	0.32	0.07	21.9	0.03	9.2	0.02	5.7	0.84	163

*Abs. and Frac. indicate absolute and fractional changes, respectively. AAOD = absorbing aerosol optical depth, BC = black carbon aerosol, DRE = direct radiative effect, DREC = clear-sky DRE, SOAG = secondary organic aerosol precursor gases.

burden and induced AAOD are tripled when a scaling factor of 3 is applied onto the BC emissions (Table 2), while BC radiative effects are increased by about 1.6 times. BC lifetime shows much less sensitivity to BC emission rates.

An increase in monolayer number from 3 to 8 and a corresponding reduction in the BC aging rate result in a higher BC burden (Figure 5a), globally about 23.8% increase in atmospheric BC amount in the model. The global mean BC lifetime can be estimated as the ratio between total BC burden and its total sinking rate including wet-scavenging and dry deposition. We find that BC lifetime is prolonged by 22.3% in M8. The less efficient wet removal is the major reason to explain the lifetime change when BC stays fresh and hydrophobic for a longer time. Increases in BC burden mainly occur near East and South Asia, Europe, central Africa, and their downwind regions (e.g., northwest Pacific and central Atlantic), indicating the coexistence of pollutants and BC as well as high potential of BC aging. In contrast, relatively pristine regions like South America also produce large amounts of BC from biomass burning but show little sensitivity to the aging efficiency. AAOD due to BC is enhanced by 20.0%, with the most significant increase in East Asia and Central Africa (Figure 5b).

The enhancement of radiative heating in the atmosphere closely follows the increase in BC concentration in M8 with a consistent spatial pattern (Figure 5c). The global mean DRE increases from 0.46 to 0.58 W/m^2 , a +26.1% fractional change. Interestingly, the geospatial pattern of DRE in the clear-sky condition is different

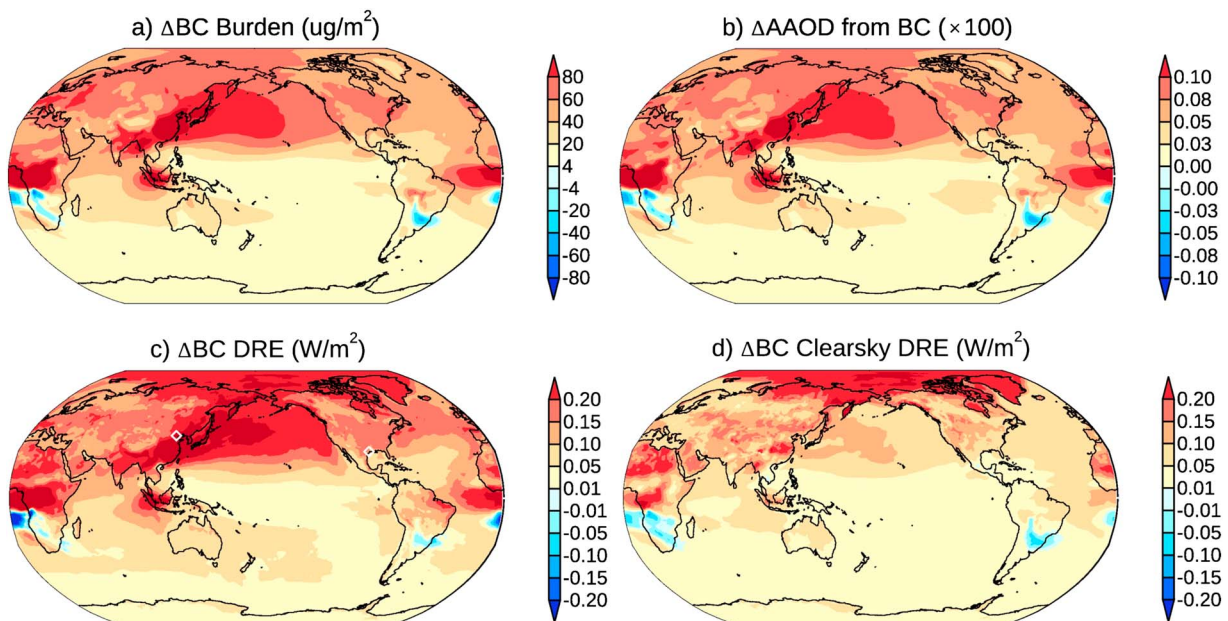


Figure 5. CAM5-MAM4 simulated changes in black carbon aerosol (BC) (a) burden in the atmosphere, (b) absorbing aerosol optical depth (AAOD), (c) direct radiative effect (DRE), and (d) DRE at clear-sky conditions from three-monolayer (M3) to eight-monolayer (M8) configurations (M8–M3).

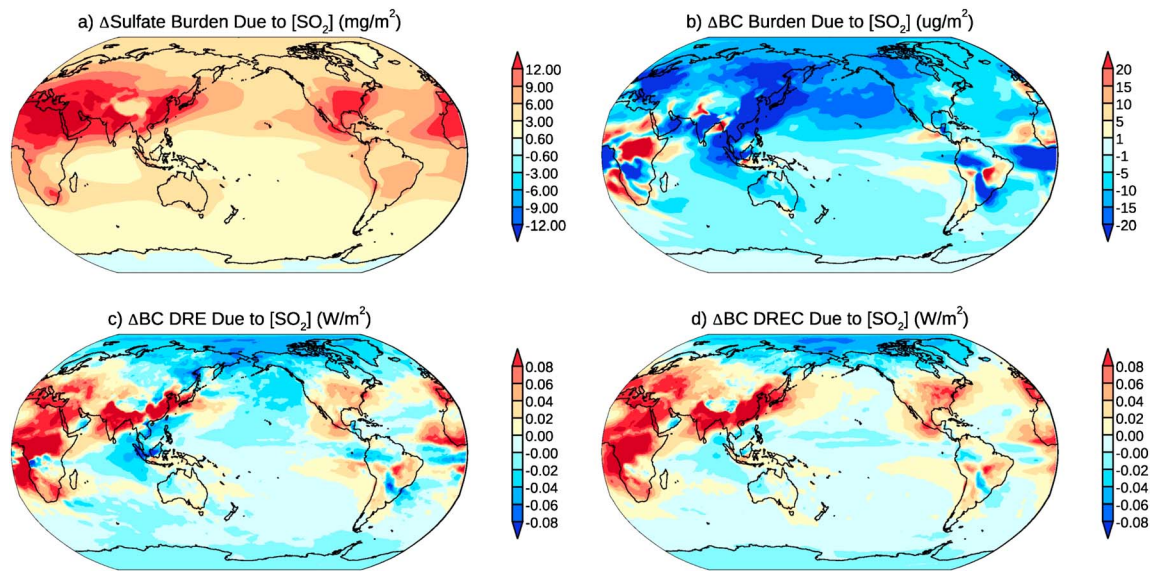


Figure 6. Aerosol burden and black carbon aerosol (BC) forcing changes due to elevation of SO_2 emission rates by a factor of 3 in CAM5-MAM4. DRE = direct radiative effect.

from all-sky DRE. The clear-sky DRE exhibits much larger enhancement over the Arctic than the midlatitudes that are closer to the BC source regions (Figure 5d). This can be explained by the Arctic sea ice induced high surface albedo and consequent large forcing efficiency. Under the all-sky conditions when clouds are taken into account in the radiation transfer, there is even stronger enhancement of aerosol absorption by the underlying clouds over the relative dark surface (Xu et al., 2017), reducing the difference of forcing efficiency over midlatitudes and the Arctic. The significant contrast between BC clear-sky and all-sky DRE implies the importance of cloud representation in GCM even for the BC direct forcing assessment, let along the indirect and semidirect forcing. Comparing the MAM3 (M0) and default MAM4 (M8), the relative increase can be even higher, about +40.1%. The large relative changes in BC burden and DRE suggest that the treatment of BC aging processes is crucial to accurately assess BC radiative effect. The difference of BC effective radiation flux at TOA between M8 and M3 is only 0.03 W/m^2 , much smaller than the BC DRE differences, implying some negative radiative effects are at play induced by the change in BC aging rate. Following the forcing

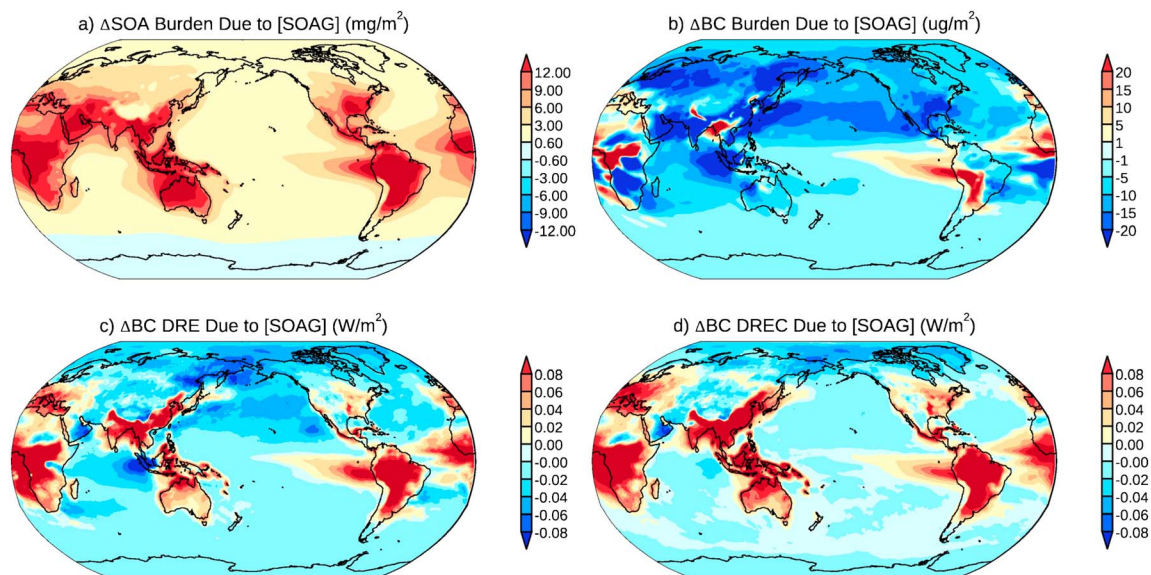


Figure 7. Same with Figure 6 but for secondary organic aerosol precursor gas (SOAG) emissions.

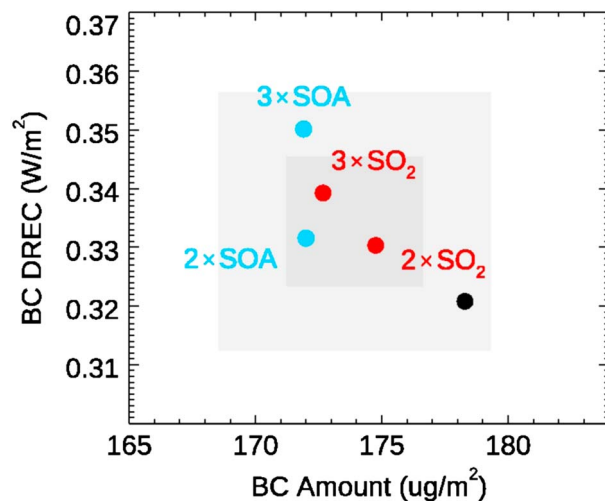


Figure 8. Global mean black carbon aerosol (BC) burden and clear-sky direct radiative effect (DREC) under different emission perturbations. The gray (light gray) box indicates the one (two) standard deviation of the five experiments as an ensemble.

decomposition method introduced by Ghan et al. (2012), we find about -0.07 W/m^2 change in the sum of indirect and semi-DRE from M3 to M8. The sign of BC semi-DRE was traditionally thought as positive, the same with BC DRE (Jacobson, 2012). However, a recent multiple climate model intercomparison study by Stjern et al. (2017) suggest the potentially large uncertainty associated with BC effect on cloud fraction ($-0.17 \pm 0.34\%$ in response to nine times BC heating), as low clouds may increase with a stabilized atmosphere.

3.3. Influence of Simulated Coating Material

Accuracy of a modeling assessment of BC DRE is subject to simulated aerosol compositions that significantly affect the BC lifetime and radiative properties of the mixture. It is well known that ground-level aerosol amounts in CAM5 are largely underestimated, especially in the heavy pollution centers like East China, their downwind regions like northwest Pacific (Wang et al., 2015), and the remote areas like the Arctic (Wang et al., 2018). Lack of aqueous phase SO_2 oxidation in aerosol water (Wang et al., 2016), no nitrate in the aerosol module, and simplified SOA formation mechanisms (Fan et al., 2018) are considered as the major reasons for the aerosol underestimation in CAM5. To examine to what extent

the biases in aerosol burden affect the BC DRE, we conduct a series of sensitivity experiments by doubling or tripling the global SO_2 and SOA precursor gases (SOAG) separately.

As shown in Figures 6a and 6b, increases in sulfate concentration results in the significant BC burden reductions over the Northern Hemisphere middle and high latitudes. Adding more coating materials tends to enhance the total hygroscopicity of BC-containing particles and reduce BC lifetime. Figure 6b also shows some regions with increases in BC amount, presumably due to the altered precipitation efficiency and atmospheric circulation after more sulfate is introduced over different regions. Globally, a three-time SO_2 emission increase results in a 3.4% decrease in BC burden in the atmosphere. Contrary to that, the BC DRE and clear-sky DRE (DREC) is enhanced by 2.4% and 5.7%, respectively. Those apparent contradictions can be explained by augmented absorption of BC particles with additional coating. The so called “lensing” effect offsets the influence of the BC mass loss, contributing to a net increase in BC DRE. Even though the global mean changes in BC burden and DRE due to the variation of coating aerosol species are generally less than 10% (Table 2), their regional changes can be up to 30%. The largest relative BC burden change due to SO_2 occurs in the Arctic, mainly because the Arctic has quite low BC background concentration but also large sensitivity to the long-range transport of BC. Also in the Arctic, the enhanced radiative absorption of aerosol particles cannot compensate the loss of BC in the atmosphere, leading to a local reduction of BC DRE (Figures 6c and 6d). Interestingly, the spatial correlation between the changes in BC DRE (Figure 6c) and sulfate burden (Figures 6a) is even higher than that between the changes in BC DRE and BC burden (Figure 6b). It implies that the BC optical properties can be a more important factor than BC burden/lifetime in regulating BC DRE. Another set of sensitivity experiment that perturb secondary organic aerosol precursor gas emissions show the similar results in Figure 7.

In comparison of one-time, two-time, and three-time emission perturbation experiments for both SO_2 and secondary organic aerosol precursor gases, Figure 8 shows that the BC property changes due to variations in non-BC aerosol species are monotonic. Taking those sensitivity experiments into one ensemble assessment, we show that BC clear-sky DRE in CAM5-MAM4 is about $0.33 \pm 0.01 \text{ W/m}^2$. Here we want to focus on clear sky rather than all-sky DRE to examine the radiative effect sensitivity, because the latter quantity is highly affected by cloud changes due to aerosol indirect effect when either sulfate or SOA concentration is elevated.

4. Conclusion and Discussion

We capitalize the field experiments of BC transformation using an ambient smoke chamber to constrain the number of coating monolayer as part of the of BC aging parameterization in MAM4 of the CAM5-Chem

model. We configure the model to mimic the chemical and physical processes in the smoke chamber deployed during two field campaigns, April to May 2009 in Houston and August to October, 2013, in Beijing. One major deficiency in the CAM5 simulation is the large bias in the aerosol burden and chemical compositions. To address this issue and facilitate a more realistic model-observation comparison, we adopt a scaling factor based on the differences between modeled and observed BC to OM ratios. The feasibility of such a scaling factor can be confirmed by the numerical equations associated with BC aging tendency in MAM4. We find that the simulated BC aging timescale with three monolayers shows better agreement with the chamber measurements. The recalibrated CAM5-MAM4 model shows a factor of 1.5–3.5 enhancement of specific absorption globally due to BC aging, especially near the BC and pollution coexisting regions.

The BC DRE can vary up to 30% due to the uncertainty in the BC aging treatment like the monolayer choice. Ghan et al. (2012) found that the different assumptions about mixing state of freshly emitted black carbon (external mixing in MAM7 and internal mixing in the accumulation mode in MAM3) produce 10% differences in BC DRE near the BC source region. Here we show that the different choices of monolayer number for the externally mixed fresh BC can produce a much larger difference. The additional coating from sulfate or SOA can reduce BC burden but enhance absorption, still resulting in a net increase in positive DRE of BC. For example, an increase in SOA formation by a factor of 3 leads to about 10% increase in BC clear-sky DRE globally. This modeling result lends help to reconcile the debate on the relative importance of increased absorption and reduced lifetime during BC aging (Boucher et al., 2016). The spatial patterns of BC forcing changes do not closely follow the changes in BC burden, indicating the importance of radiative properties of BC-containing particles (Tian et al., 2017) and distinctive forcing efficiency over different regions.

Our analyses suggest that the BC forcing assessment is largely determined by both aging parameterization and modeled concentrations of both BC and coating aerosol species. Currently, the large biases still exist in the BC emission inventory. Even though the CMIP6 anthropogenic emissions of BC from Community Emissions Data System (Hoesly et al., 2018) get improved compared with those used in CMIP5, we find even lower total BC burden (6% reduction) using the CMIP6 emission in the CAM5-MAM4 simulation, mainly due to the uncertainty in predicting the injection height of biomass burning aerosols. The latest CESM2 with CMIP6 largely confines the biomass burning-BC emission to the surface level, which makes BC more easily removed by dry/wet deposition. Meanwhile, simulated total aerosol concentration and relative fraction for each component are other important sources of uncertainty with BC radiative effect and their effects on the climate. An observationally based aerosol composition data set with global coverage that provides the mass concentration of different aerosol species would be useful. Moreover, since our results show that the BC aging characteristics have a large regional variability, this study also suggests that a chamber measurement campaign at various locations is needed for constraining GCMs.

Acknowledgments

Y. Wang and J. H. Jiang appreciate the support by the NASA ROSES ACMAP and CCST programs and the support from the Jet Propulsion Laboratory, California Institute of Technology, under a contract with the National Aeronautics and Space Administration. Y. Wang and Y. L. Yung appreciate the support by the NSF (award 1700727). P.-L. Ma acknowledges the internal support from the Pacific Northwest National Laboratory, which is operated for the Department of Energy by Battelle Memorial Institute under contract DE-AC05-76RL01830. The CESM source code can be obtained from <http://www.cesm.ucar.edu/>. All model and chamber experiment results are stored at our FTP server at California Institute of Technology and available upon request. Please contact Yuan Wang (yuan.wang@caltech.edu) to access those data.

References

- Bond, T. C., & Bergstrom, R. W. (2006). Light absorption by carbonaceous particles: An investigative review. *Aerospace Science and Technology*, 40(1), 27–67. <https://doi.org/10.1080/02786820500421521>
- Bond, T. C., Doherty, S. J., Fahey, D. W., Forster, P. M., Berntsen, T., DeAngelo, B. J., et al. (2013). Bounding the role of black carbon in the climate system: A scientific assessment. *Journal of Geophysical Research: Atmospheres*, 118, 5380–5552. <https://doi.org/10.1002/jgrd.50171>
- Boucher, O., Balkanski, Y., Hodnebrog, O., Myhre, C. L., Myhre, G., Quaas, J., et al. (2016). Jury is still out on the radiative forcing by black carbon. *Proceedings of the National Academy of Sciences of the United States of America*, 113(35), E5092–E5093. <https://doi.org/10.1073/pnas.1607005113>
- Cappa, C. D., Onasch, T. B., Massoli, P., Worsnop, D. R., Bates, T. S., Cross, E. S., et al. (2012). Radiative absorption enhancements due to the mixing state of atmospheric black carbon. *Science*, 337(6098), 1078–1081. <https://doi.org/10.1126/science.1223447>
- Chen, B., Bai, Z., Cui, X., Chen, J., Andersson, A., & Gustafsson, O. (2017). Light absorption enhancement of black carbon from urban haze in northern China winter. *Environmental Pollution*, 221, 418–426. <https://doi.org/10.1016/j.envpol.2016.12.004>
- Chin, M., Diehl, T., Dubovik, O., Eck, T. F., Holben, B. N., Sinyuk, A., et al. (2009). Light absorption by pollution, dust, and biomass burning aerosols: A global model study and evaluation with AERONET measurements. *Annales Geophysicae-Germany*, 27(9), 3439–3464. <https://doi.org/10.5194/angeo-27-3439-2009>
- Fan, T., Liu, X., Ma, P. L., Zhang, Q., Li, Z., Jiang, Y., et al. (2018). Emission or atmospheric processes? An attempt to attribute the source of large bias of aerosols in eastern China simulated by global climate models. *Atmospheric Chemistry and Physics*, 18(2), 1395–1417. <https://doi.org/10.5194/acp-18-1395-2018>
- Forster, P. M., Richardson, T., Maycock, A. C., Smith, C. J., Samset, B. H., Myhre, G., et al. (2016). Recommendations for diagnosing effective radiative forcing from climate models for CMIP6. *Journal of Geophysical Research: Atmospheres*, 121, 12,460–12,475. <https://doi.org/10.1002/2016jd025320>
- Ghan, S. J., Liu, X., Easter, R. C., Zaveri, R., Rasch, P. J., Yoon, J. H., & Eaton, B. (2012). Toward a minimal representation of aerosols in climate models: Comparative decomposition of aerosol direct, semidirect, and indirect radiative forcing. *Journal of Climate*, 25(19), 6461–6476. <https://doi.org/10.1175/jcli-d-11-00650.1>

- Ghan, S. J., & Zaveri, R. A. (2007). Parameterization of optical properties for hydrated internally mixed aerosol. *Journal of Geophysical Research*, *112*, D10201. <https://doi.org/10.1029/2006JD007927>
- Guo, S., Hu, M., Zamora, M. L., Peng, J., Shang, D., Zheng, J., et al. (2014). Elucidating severe urban haze formation in China. *Proceedings of the National Academy of Sciences of the United States of America*, *111*(17), 17,373–17,378.
- Gustafsson, O., & Ramanathan, V. (2016). Convergence on climate warming by black carbon aerosols. *Proceedings of the National Academy of Sciences of the United States of America*, *113*(16), 4243–4245. <https://doi.org/10.1073/pnas.1603570113>
- He, C., Liou, K. N., Takano, Y., Zhang, R., Levy Zamora, M., Yang, P., et al. (2015). Variation of the radiative properties during black carbon aging: Theoretical and experimental intercomparison. *Atmospheric Chemistry and Physics*, *15*(20), 11,967–11,980. <https://doi.org/10.5194/acp-15-11967-2015>
- Hoesly, R. M., Smith, S. J., Feng, L., Klimont, Z., Janssens-Maenhout, G., Pitkanen, T., et al. (2018). Historical (1750–2014) anthropogenic emissions of reactive gases and aerosols from the Community Emissions Data System (CEDS). *Geoscientific Model Development*, *11*(1), 369–408. <https://doi.org/10.5194/gmd-11-369-2018>
- Hu, W., Hu, M., Hu, W.-W., Zheng, J., Chen, C., Wu, Y., & Guo, S. (2017). Seasonal variations in high time-resolved chemical compositions, sources, and evolution of atmospheric submicron aerosols in the megacity Beijing. *Atmospheric Chemistry and Physics*, *17*(16), 9979–10,000. <https://doi.org/10.5194/acp-17-9979-2017>
- Jacobson, M. Z. (2001). Strong radiative heating due to the mixing state of black carbon in atmospheric aerosols. *Nature*, *409*(6821), 695–697. <https://doi.org/10.1038/35055518>
- Jacobson, M. Z. (2012). Investigating cloud absorption effects: Global absorption properties of black carbon, tar balls, and soil dust in clouds and aerosols. *Journal of Geophysical Research*, *117*, D06205. <https://doi.org/10.1029/2011JD017218>
- Jiang, Y., Lu, Z., Liu, X., Qian, Y., Zhang, K., Wang, Y., & Yang, X. Q. (2016). Impacts of global open-fire aerosols on direct radiative, cloud and surface-albedo effects simulated with CAM5. *Atmospheric Chemistry and Physics*, *16*(23), 14,805–14,824. <https://doi.org/10.5194/acp-16-14805-2016>
- Khalizov, A. F., Xue, H., & Zhang, R. (2009). Enhanced light absorption and scattering by carbon soot aerosols internally mixed with sulfuric acid. *The Journal of Physical Chemistry*, *113*(6), 1066–1074. <https://doi.org/10.1021/jp807531n>
- Koch, D., Schulz, M., Kinne, S., McNaughton, C., Spackman, J. R., Balkanski, Y., et al. (2009). Evaluation of black carbon estimations in global aerosol models. *Atmospheric Chemistry and Physics*, *9*(22), 9001–9026. <https://doi.org/10.5194/acp-9-9001-2009>
- Laborde, M., Crippa, M., Tritscher, T., Jurányi, Z., Decarlo, P. F., Temime-Roussel, B., et al. (2013). Black carbon physical properties and mixing state in the European megacity Paris. *Atmospheric Chemistry and Physics*, *13*(11), 5831–5856. <https://doi.org/10.5194/acp-13-5831-2013>
- Lamarque, J. F., Bond, T. C., Eyring, V., Granier, C., Heil, A., Klimont, Z., et al. (2010). Historical (1850–2000) gridded anthropogenic and biomass burning emissions of reactive gases and aerosols: Methodology and application. *Atmospheric Chemistry and Physics*, *10*(15), 7017–7039. <https://doi.org/10.5194/acp-10-7017-2010>
- Levy, M. E., Zhang, R., Khalizov, A. F., Zheng, J., Collins, D. R., Glen, C. R., et al. (2013). Measurements of submicron aerosols in Houston, Texas during the 2009 SHARP field campaign. *Journal of Geophysical Research: Atmospheres*, *118*, 10,518–10,534. <https://doi.org/10.1002/jgrd.50785>
- Liu, D., Flynn, M., Gysel, M., Targino, A., Crawford, I., Bower, K., et al. (2010). Single particle characterization of black carbon aerosols at a tropospheric alpine site in Switzerland. *Atmospheric Chemistry and Physics*, *10*(15), 7389–7407. <https://doi.org/10.5194/acp-10-7389-2010>
- Liu, D., Whitehead, J., Alfara, M. R., Reyes-Villegas, E., Spracklen, D. V., Reddington, C. L., et al. (2017). Black-carbon absorption enhancement in the atmosphere determined by particle mixing state. *Nature Geoscience*, *10*(3), 184–188. <https://doi.org/10.1038/ngeo2901>
- Liu, X., Easter, R. C., Ghan, S. J., Zaveri, R., Rasch, P., Shi, X., et al. (2012). Toward a minimal representation of aerosols in climate models: Description and evaluation in the Community Atmosphere Model CAM5. *Geoscientific Model Development*, *5*(3), 709–739. <https://doi.org/10.5194/gmd-5-709-2012>
- Liu, X., Ma, P. L., Wang, H., Tilmes, S., Singh, B., Easter, R. C., et al. (2016). Description and evaluation of a new four-mode version of the Modal Aerosol Module (MAM4) within version 5.3 of the Community Atmosphere Model. *Geoscientific Model Development*, *9*(2), 505–522. <https://doi.org/10.5194/gmd-9-505-2016>
- Liu, X., Penner, J. E., Das, B., Bergmann, D., Rodriguez, J. M., Strahan, S., et al. (2007). Uncertainties in global aerosol simulations: Assessment using three meteorological datasets. *Journal of Geophysical Research*, *112*, D11212. <https://doi.org/10.1029/2006JD008216>
- Ma, P.-L., Rasch, P. J., Wang, M., Wang, H., Ghan, S. J., Easter, R. C., et al. (2015). How does increasing horizontal resolution in a global climate model improve the simulation of aerosol-cloud interactions? *Geophysical Research Letters*, *42*, 5058–5065. <https://doi.org/10.1002/2015GL064183>
- Neale, R., Chen, C. C., Gettelman, A., Lauritzen, P., Park, S., Williamson, D. L., et al. (2012). *Description of the NCAR Community Atmosphere Model (CAM 5.0)* (NCAR Technical Note NCAR/TN-486+STR). Boulder, CO: National Center for Atmospheric Research (NCAR). http://www.cesm.ucar.edu/models/cesm1.0/cam/docs/description/cam5_desc.pdf
- Olague, E. P., Kolb, C. E., Lefer, B., Rappenglück, B., Zhang, R., & Pinto, J. P. (2014). Overview of the SHARP campaign: Motivation, design, and major outcomes. *Journal of Geophysical Research: Atmospheres*, *119*, 2597–2610. <https://doi.org/10.1002/2013jd019730>
- Peng, J., Hu, M., Guo, S., du, Z., Shang, D., Zheng, J., et al. (2017). Ageing and hygroscopicity variation of black carbon particles in Beijing measured by a quasi-atmospheric aerosol evolution study (QUALITY) chamber. *Atmospheric Chemistry and Physics*, *17*(17), 10,333–10,348. <https://doi.org/10.5194/acp-17-10333-2017>
- Peng, J., Hu, M., Guo, S., du, Z., Zheng, J., Shang, D., et al. (2016). Markedly enhanced absorption and direct radiative forcing of black carbon under polluted urban environments. *Proceedings of the National Academy of Sciences of the United States of America*, *113*(16), 4266–4271. <https://doi.org/10.1073/pnas.1602310113>
- Samset, B. H., Stjern, C. W., Andrews, E., Kahn, R. A., Myhre, G., Schulz, M., & Schuster, G. L. (2018). Aerosol Absorption: Progress Towards Global and Regional Constraints. *Current Climate Change Reports*, *4*(2), 65–83. <https://doi.org/10.1007/s40641-018-0091-4>
- Stjern, C. W., Samset, B. H., Myhre, G., Forster, P. M., Hodnebrog, Ø., Andrews, T., et al. (2017). Rapid adjustments cause weak surface temperature response to increased black carbon concentrations. *Journal of Geophysical Research: Atmospheres*, *122*, 11,462–11,481. <https://doi.org/10.1002/2017JD027326>
- Thamban, N. M., Tripathi, S. N., Moosakutty, S. P., Kuntamukkala, P., & Kanawade, V. P. (2017). Internally mixed black carbon in the Indo-Gangetic Plain and its effect on absorption enhancement. *Atmospheric Research*, *197*, 211–223. <https://doi.org/10.1016/j.atmosres.2017.07.007>
- Tian, P., Cao, X., Zhang, L., Sun, N., Sun, L., Logan, T., et al. (2017). Aerosol vertical distribution and optical properties over China from long-term satellite and ground-based remote sensing. *Atmospheric Chemistry and Physics*, *17*(4), 2509–2523. <https://doi.org/10.5194/acp-17-2509-2017>

- Tie, X., Madronich, S., Walters, S., Edwards, D., Ginoux, P., Mahowald, N., et al. (2005). Assessment of global impact of aerosols on tropospheric oxidants. *Journal of Geophysical Research*, *110*, D03204. <https://doi.org/10.1029/2004JD005359>
- Tilmes, S., Lamarque, J. F., Emmons, L. K., Kinnison, D. E., Ma, P. L., Liu, X., et al. (2015). Description and evaluation of tropospheric chemistry and aerosols in the Community Earth System Model (CESM1.2). *Geoscientific Model Development*, *8*(5), 1395–1426. <https://doi.org/10.5194/gmd-8-1395-2015>
- Wang, G., Zhang, R., Gomez, M. E., Yang, L., Levy Zamora, M., Hu, M., et al. (2016). Persistent sulfate formation from London fog to Chinese haze. *Proceedings of the National Academy of Sciences of the United States of America*, *113*(48), 13,630–13,635. <https://doi.org/10.1073/pnas.1616540113>
- Wang, R., Andrews, E., Balkanski, Y., Boucher, O., Myhre, G., Samset, B. H., et al. (2018). Spatial representativeness error in the ground-level observation networks for black carbon radiation absorption. *Geophysical Research Letters*, *45*, 2106–2114. <https://doi.org/10.1002/2017GL076817>
- Wang, Y., Jiang, J. H., & Su, H. (2015). Atmospheric responses to the redistribution of anthropogenic aerosols. *Journal of Geophysical Research: Atmospheres*, *120*, 9625–9641. <https://doi.org/10.1002/2015jd023665>
- Wang, Y., Khalizov, A., Levy, M., & Zhang, R. (2013). New directions: Light absorbing aerosols and their atmospheric impacts. *Atmospheric Environment*, *81*, 713–715. <https://doi.org/10.1016/j.atmosenv.2013.09.034>
- Xu, H., Guo, J., Wang, Y., Zhao, C., Zhang, Z., Min, M., et al. (2017). Warming effect of dust aerosols modulated by overlapping clouds below. *Atmospheric Environment*, *166*, 393–402. <https://doi.org/10.1016/j.atmosenv.2017.07.036>
- Xu, Y., & Xie, S.-P. (2015). Ocean mediation of tropospheric response to reflecting and absorbing aerosols. *Atmospheric Chemistry and Physics*, *15*(10), 5827–5833. <https://doi.org/10.5194/acp-15-5827-2015>
- Xue, H., Khalizov, A. F., Wang, L., Zheng, J., & Zhang, R. (2009). Effects of dicarboxylic acid coating on the optical properties of soot. *Physical Chemistry Chemical Physics*, *11*, 7865–7875. <https://doi.org/10.1039/b700001a>
- Zanatta, M., Gysel, M., Bukowiecki, N., Müller, T., Weingartner, E., Areskou, H., et al. (2016). A European aerosol phenomenology-5: Climatology of black carbon optical properties at 9 regional background sites across Europe. *Atmospheric Environment*, *145*, 346–364. <https://doi.org/10.1016/j.atmosenv.2016.09.035>
- Zhang, R., Wang, G., Guo, S., Zamora, M. L., Ying, Q., Lin, Y., et al. (2015). Formation of urban fine particulate matter. *Chemical Reviews*, *115*(10), 3803–3855. <https://doi.org/10.1021/acs.chemrev.5b00067>
- Zhang, R. Y., Khalizov, A. F., Pagels, J., Zhang, D., Xue, H. X., & McMurry, P. H. (2008). Variability in morphology, hygroscopicity, and optical properties of soot aerosols during atmospheric processing. *Proceedings of the National Academy of Sciences of the United States of America*, *105*(30), 10,291–10,296. <https://doi.org/10.1073/pnas.0804860105>